Multiwavelength Spectral Studies Of Fermi-LAT Blazars

Authors: M. Joshi, S. Jorstad, A. Marscher (Boston U.), M. Böttcher (Ohio U.), I. Agudo (Boston U. & IAA), V. Larionov (St. Petersburg State U.), M. Aller (U. Michigan), M. Gurwell (SAO), A.Lahteenmaki (Metsahovi Obs.), P. Smith (Steward Obs.)

Abstract: We present ϒ-ray, x-ray, and optical (photometric & polarimetric in R band) lightcurves (lcs) of Fermi-LAT blazar, 3C279, which is part of the Boston University multiwaveband polarization monitoring program. Data have been compiled from observations with Fermi, Swift, RXTE, VLBA, & various ground-based optical and radio telescopes. We simulate dynamic spectral energy distribution (SEDs) of 3C279, observed on 01/15/2006, within the framework of a multi-slice, time-dependent leptonic jet model for blazars, with radiation feedback, in internal shock scenario. We use physical jet parameters obtained from VLBA monitoring to guide our modeling efforts. We discuss the role of intrinsic parameters and interplay between synchrotron & inverse Compton (Synchrotron Self Compton, SSC or External Compton, EC) radiation processes responsible for producing the resultant SEDs.

Motivation:

Blazar jets are highly violent in nature and are dominated by ultrarelativistic particles.

- SED of blazars consists of low-energy component due to synchrotron radiation emanating from relativistic particles; high-energy component (for leptonic jet model) due to Compton upscattering of the seed photon field (SSC or EC) by ultrarelativistic particles [1].
- Mode of acceleration of particles to high energies and its location in jet not completely understood.
- Internal shock model could be used to comprehend the physics of particle acceleration. In this model,
  - central engine (black hole + accretion disk) ejects plasma shells of different velocity, mass, & energy
  - collision between shells gives rise to internal shocks (reverse (RS) and forward (FS))
  - shocks convert ordered bulk kinetic energy of plasma into magnetic field energy and random kinetic energy of particles
  - highly accelerated particles radiate & produce emission observed from the jet

Current Work:

Model of [2] used to analyze SED of 3C279, observed on 01/15/2006 in its optical high state, & jet parameters from VLBA monitoring [4] used to form initial set of input parameters. ϒ-ray lcs of 3C279 obtained using Fermi-LAT from 08/2008 - 03/2011 are shown, & 2 one-month time periods (F1: 11/08 - 12/08/2008; & Q1: 05/22 - 06/26/2010) have been extracted corresponding to a flaring & quiescent episode, resp.

☐We present X-ray (Swift & RXTE), optical (R-band), & polarization (R-band & VLBI) data for F1 & Q1 & show their SEDs to gain insight on the evolution of its SEDs over longer time periods.

Internal Shock Model:

Collision of two plasma shells results in an emission region as shown in Fig. 1. Treatment of shell collision and shock propagation is hydrodynamic and relativistic in nature [3].

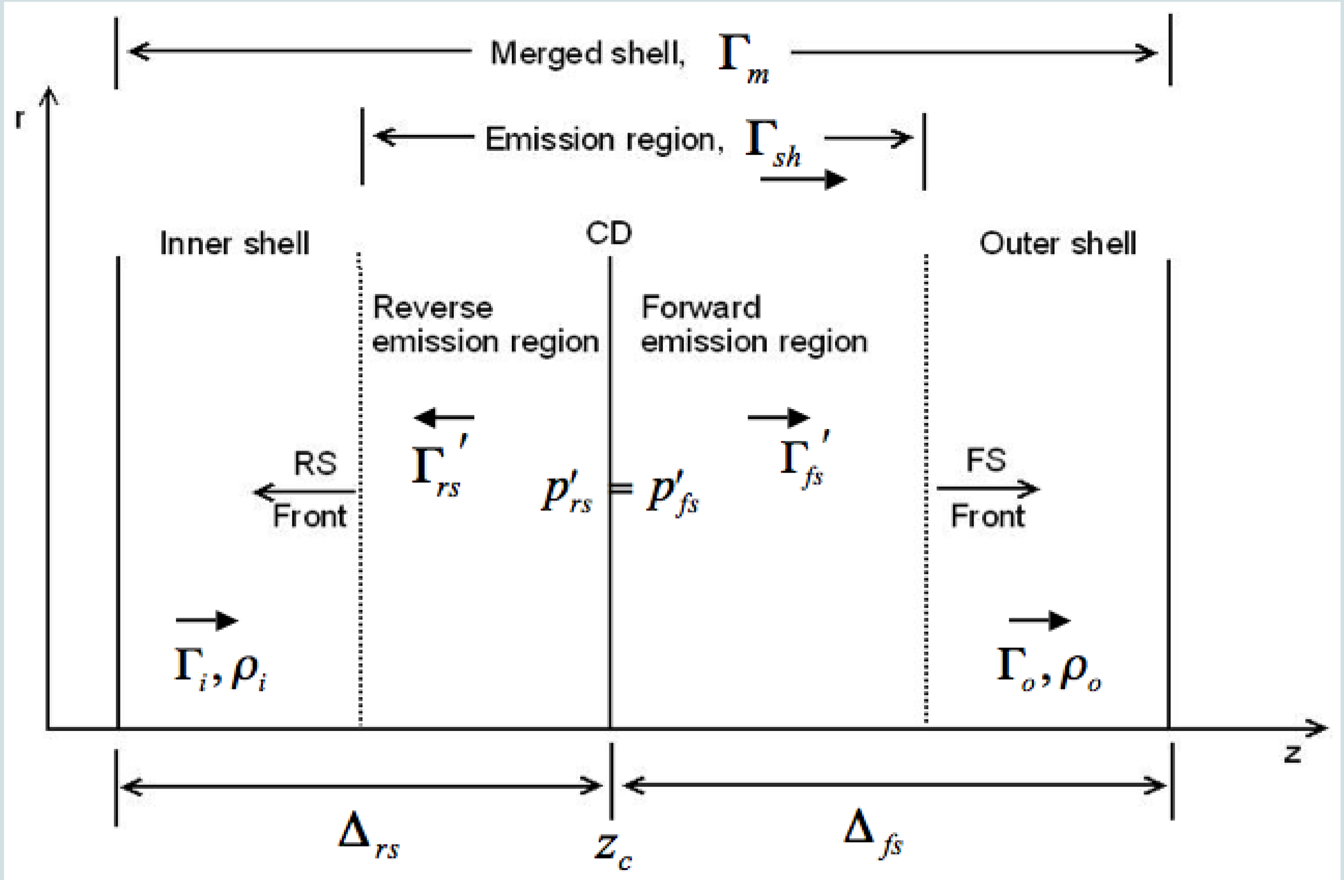

Fig. 1: Schematic of the emission region with RS traveling into the inner shell of BLF, Γ_i and FS moving into the outer shell with BLF, Γ_o ($\Gamma_i > \Gamma_o$). The pressures of the two shocked fluids, p'_{rs} & p'_{fs} are same across CD. The Δ_{rs} & Δ_{fs} are the widths of the inner and outer shell after the collision in the lab (central engine) frame obtained from the shock dynamics ([3] & [5]).

Multi-slice Radiation Transfer Scheme:

Cylindrical emission region considered to calculate resultant spectrum in a time-dependent manner. Inhomogeneity in photon and particle density throughout emission region considered by dividing the region into multiple slices (Fig. 2) [2]. Radiation transfer (Eqn. 1) considered within each slice and in between slices.

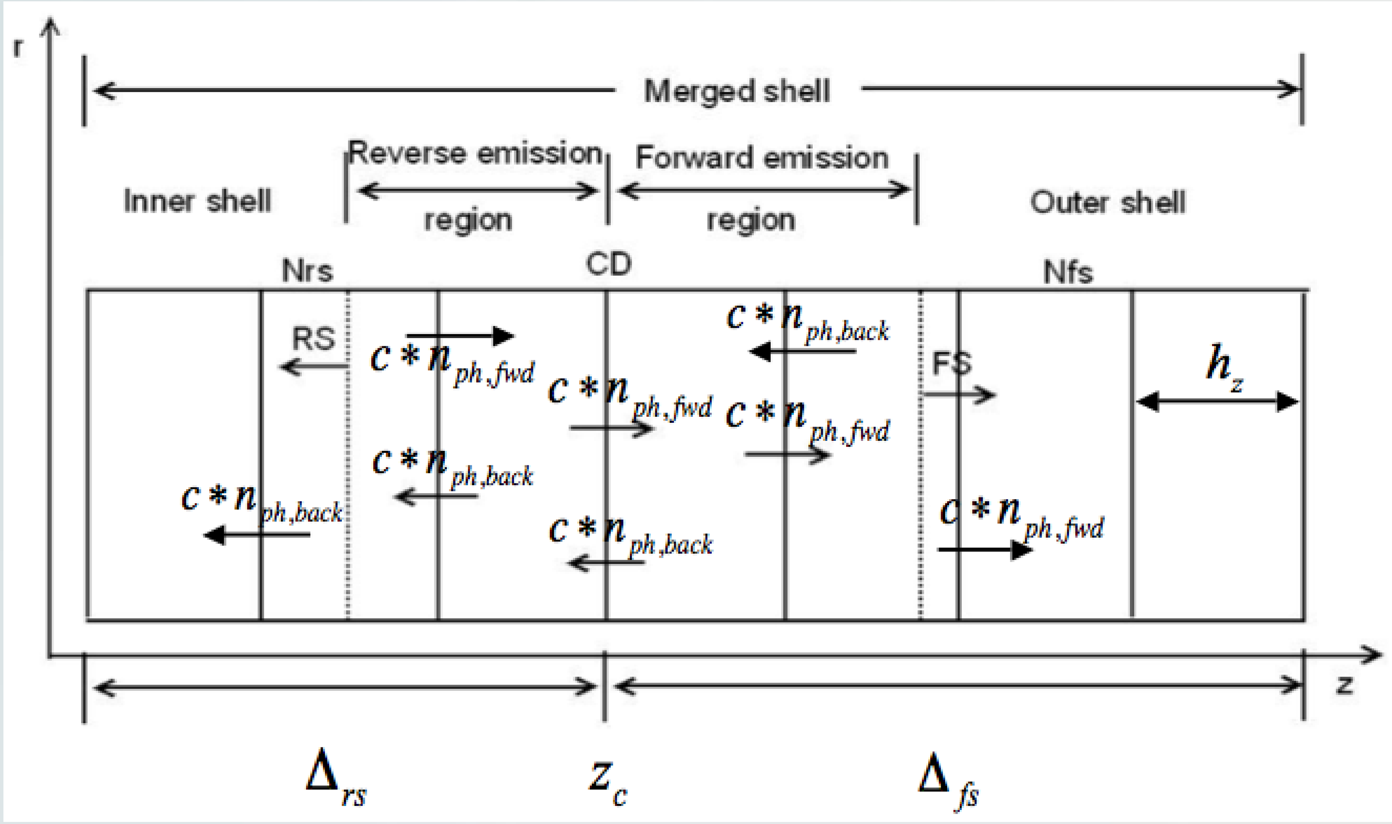

Fig. 2: Schematic of radiation transfer in between slices using photon escape probability functions.

$$dn_{ph,fwd} = n_{ph}\frac{dt}{t_{ph,esc}}P_{fwd} \quad (1)$$

Future Development of Model

- Include EC due to broad line region & dusty torus to reproduce observed SEDs.
- Include inferred orientation of the magnetic field from polarization monitoring programs.
- Study of intrinsic parameter differences between various blazar subclasses, arising from the orientation of the magnetic field in the jet.

First Results (Synchrotron + Synchrotron Self Compton):

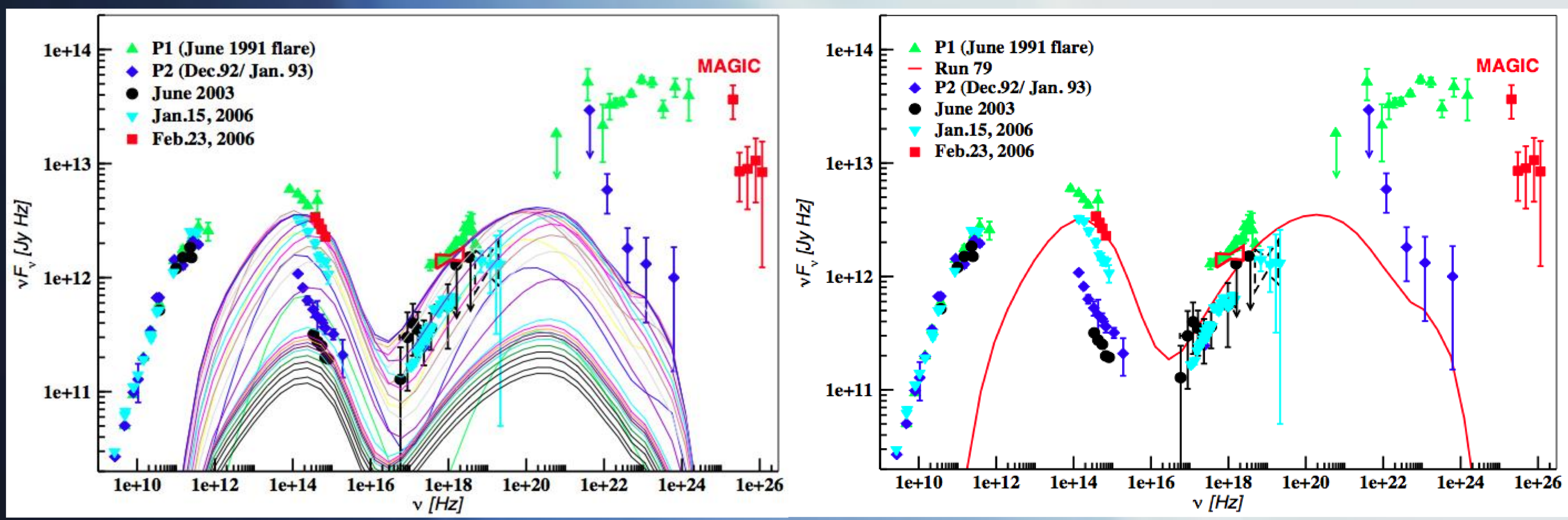

$L_{kin} \sim 7e47 ergs/s$

$R \sim 3.7e16; \Delta_i \sim 8.5e15cm$

$\Delta_o \sim 9.5e15cm; \theta_{obs} \sim 1.0^\circ$

$q \sim 4.0$

$\Gamma_{sh} \sim 16.6; B \sim 3.8G$

$\gamma_{max} \sim 4e4$

$\gamma_{min,fs} \sim 6e2; \gamma_{min,rs} \sim 1e3$

Fig. 3: Simulated instantaneous and time-integrated (averaged over 1.0 day) SED 3C279 for 01/15/2006, resulting from synchrotron and SSC processes.

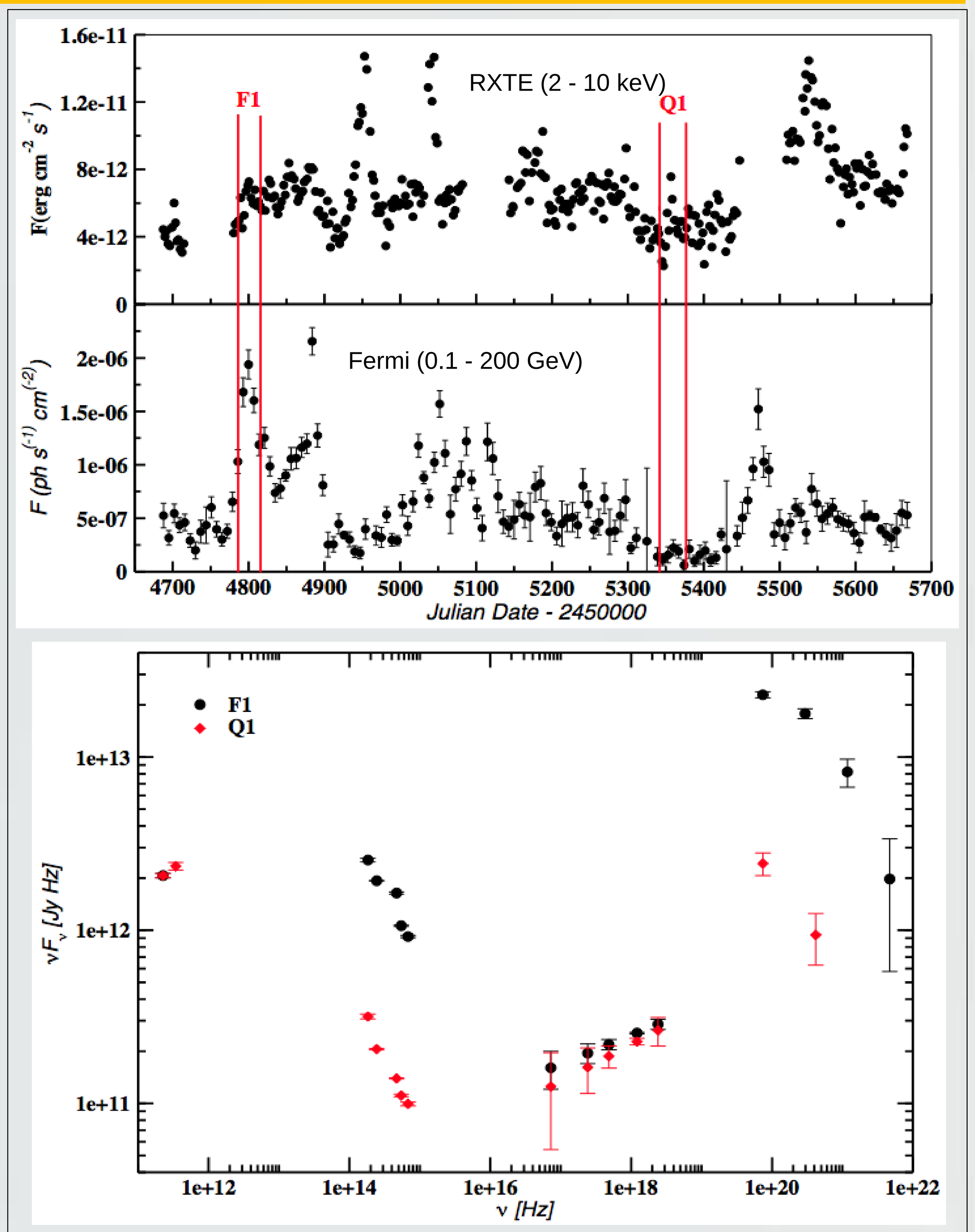

Fig. 4: Observed lightcurves from 08/09/2008 - 04/16/2011 and SED of 3C279 for periods F1 & Q1. Long-term variability as seen in the x-rays & gamma-ray. Seems to be correlation between the two wavebands that could suggest common source of origin.

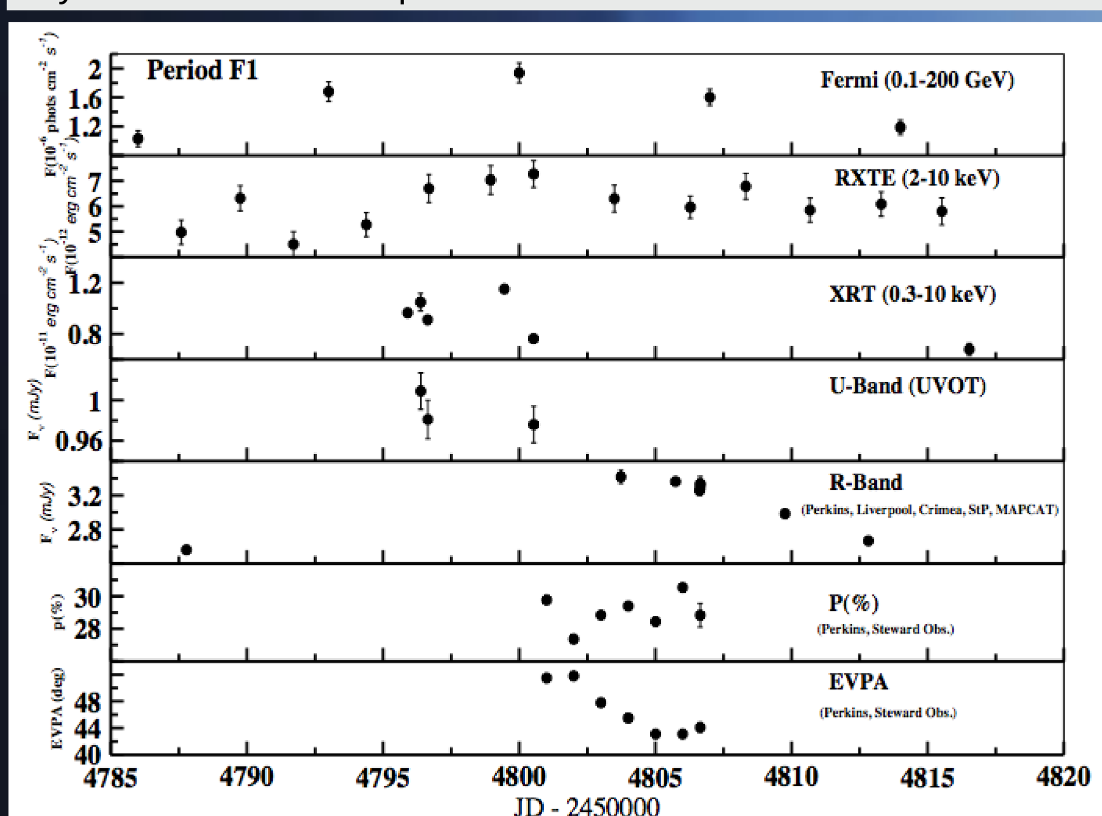

Fig. 5: Multi-waveband lightcurves for the period F1. Reasonable correlation between gamma-ray & x-ray data, x-rays last longer in flaring, as expected. But more complicated features are present for such shorter time-periods that need to be discussed in detail.

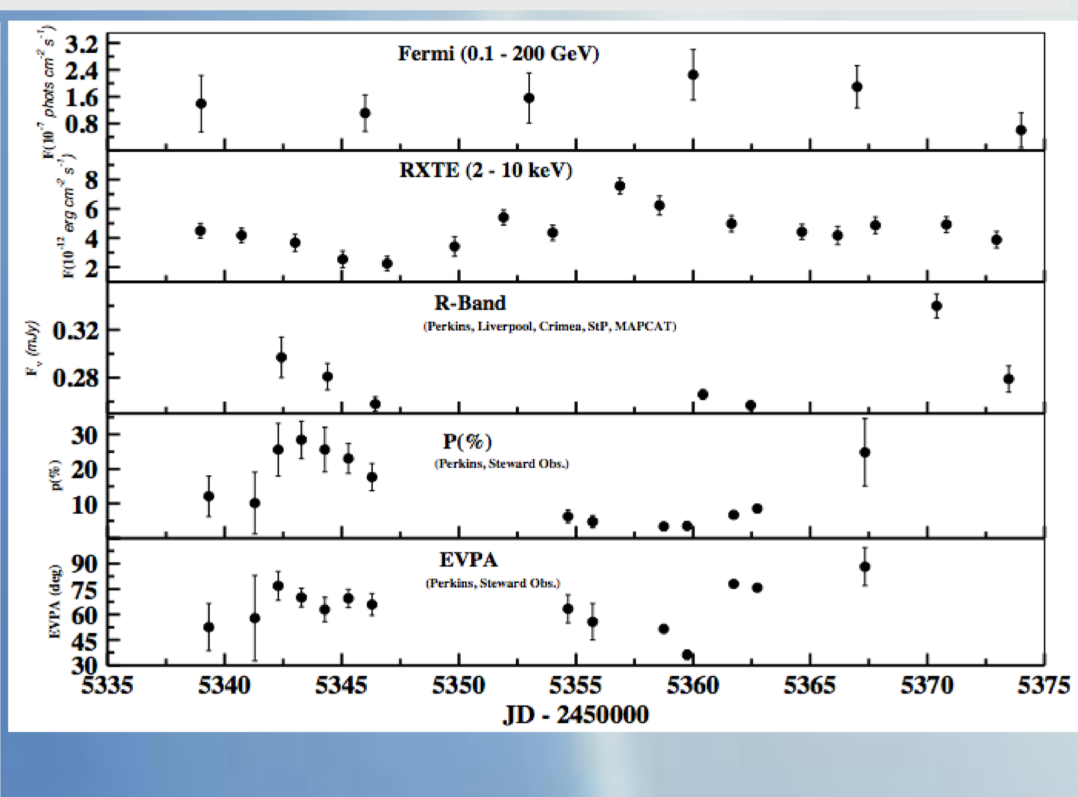

Fig. 6: R-band data seems to be in agreement with the optical polarization data. For VLBA data on 5363, p = 4.7+-0.8 & EVPA = 78.3+-4.9, which does agree very well with both the p & EVPA value in the optical. This could suggest a common source of origin for the two.

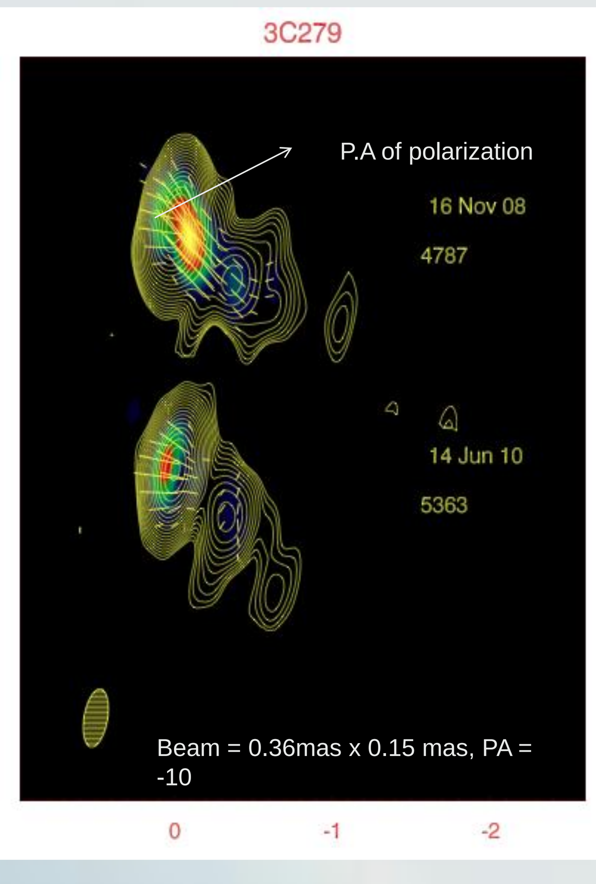

Fig. 7: Peaks of total (contours) & polarized (color scale) intensity on 11/16/2008, S_total_peak=12.0 Jy/beam & S_pol_peak = 0.47Jy/beam, on 06/14/2010 S_total_peak = 9.5 Jy/beam & S_pol_peak = 0.30Jy/beam.

[1] Böttcher & Schlickeiser, R., 1997, A&A, 325, 866.
[2] Joshi & Böttcher, 2011, ApJ, 727, 21.
[3] Spada et al., 2001, MNRAS, 325, 1559.
[4] Jorstad et al., 2005, AJ, 130, 1418.
[5] Böttcher & Dermer, 2010, ApJ, 711, 445

This research was supported in part by NASA through Fermi grants NNX10AO59G, NNX08AV65G, and NNX08AV61G, NASA through Swift grants NASA through Swift grants NNX09AR11G, NNX10AL13G, and NNX10AF88G, and by NSF grant AST-0907893.